Applied Catalysis B: Environmental 92 (2009) 307–317

Contents lists available at ScienceDirect

Applied Catalysis B: Environmental

journal homepage: www.elsevier.com/locate/apcatb

Calorimetric study of the reversibility of CO pollutant adsorption on high loaded Pt/carbon catalysts used in PEM fuel cells

Georgeta Postole [1], Simona Bennici, Aline Auroux *

Institut de Recherches sur la Catalyse et l'Environnement de Lyon, UMR 5256, CNRS-UCBLyon1, 2 av. Albert Einstein, 69626 Villeurbanne Cedex, France

ARTICLE INFO

Article history:
Received 21 June 2009
Received in revised form 27 July 2009
Accepted 3 August 2009
Available online 7 August 2009

Keywords:
Microcalorimetry
Differential heat of adsorption
Carbon monoxide
Platinum
Carbon support

ABSTRACT

A major obstacle to the broader use of fuel cells is the poisoning of supported Pt catalysts by the CO present in virtually all feeds. In this paper, the microcalorimetry technique was employed to study and compare the CO adsorption properties of different commercial carbon-supported platinum catalysts with high Pt loading, aimed to be used in proton exchange membrane fuel cells (PEMFCs) applications. Combined with other techniques of characterization, such as BET, XRD, TPD-MS and TPR, adsorption microcalorimetry has permitted a better understanding of the studied systems. The pore architecture of Pt/C catalysts was found to influence the kinetics of heat release during CO adsorption. The accessibility of CO molecules to the adsorption sites increased with the mesoporosity of the catalyst. The degree of catalyst poisoning by CO upon successive air/H_2/CO cycles varied between 2 and 30% for the different studied samples. These results confirm that the surface chemistry of the catalyst, and in particular the Pt deposition method, affects the surface site energy distribution and consequently the adsorptive properties towards H_2 and CO. It was found that both H_2 and CO are chemisorbed on the investigated samples. Pt/C powders exhibit higher differential heats of carbon monoxide adsorption in comparison with hydrogen adsorption. A reaction between pre-adsorbed H_2 and CO from the gas phase takes place on Pt/C catalysts as a result of competitive adsorption.

1. Introduction

It is universally accepted that hydrogen is one of the most promising energy carriers, as it can be used as a clean fuel in a variety of energy end-use sectors, including conversion to electricity without CO_2 emission [1–3]. Therefore its demand will greatly increase in the near future.

Proton exchange membrane fuel cells (PEMFCs) have great potential for mobile and stationary power supply applications [4,5]. The biggest advantage of PEMFCs over internal combustion engines in automotive vehicles is the absence of emissions when using hydrogen as the fuel and air as the oxidant [6]. In proton exchange membrane fuel cells, hydrogen is oxidized at the anode; free protons which appear as a result of this oxidation enter into the electrolyte and they are transported to the cathode. Such power devices operate at high efficiency when pure hydrogen is used. However, the production, storage, and refuelling infrastructure are still significant obstacles to the widespread adoption of hydrogen as a fuel [7]. To avoid such difficulties, the use of hydrogen-rich synthetic gas obtained from steam-reforming or partial oxidation of alcohols or hydrocarbons can be a feasible choice, but in this case the efficiency of PEMFCs would fail due to the presence of impurities such as CO, H_2S, NH_3, organic sulphur-carbon and carbon-hydrogen compounds in hydrogen fuel [8–11]. Using special selective oxidation catalysts, the CO concentration in hydrogen can be further reduced to approximately 2–100 ppm. But even at this level, the CO-poisoning effect could significantly affect the long-term performance of the PEMFC stack [12].

Although a huge variety of materials have been investigated, so far the most common catalyst for hydrogen/oxygen fuel cells on the anode and cathode sides is nano-dispersed platinum supported on active carbon [2,3,5,11,13]. The most important disadvantage of Pt/C materials is that their catalytic activity is negatively affected, even at low temperatures, by traces of CO present in the feedstock at concentrations as low as 10 ppm [14–17]. The CO-poisoning effect for hydrogen adsorption arises from a blocking of the surface active sites by CO, as carbon monoxide molecules are much more strongly bonded to the surface than hydrogen and the oxidation potential of adsorbed CO is much higher than that of adsorbed hydrogen [18]. The adsorbed CO not only affects the reactivity of

* Corresponding author. Tel.: +33 472 44 53 98; fax: +33 472 44 53 99.
E-mail address: aline.auroux@ircelyon.univ-lyon1.fr (A. Auroux).
[1] Permanent address: Institute of Physical Chemistry "Ilie Murgulescu" of the Romanian Academy, Spl. Independentei 202, 060021 Bucharest, Romania.

0926-3373/$ – see front matter © 2009 Elsevier B.V. All rights reserved.
doi:10.1016/j.apcatb.2009.08.009

the accessible electrode surface by preventing H_2 adsorption on the covered sites, but also lowers the reactivity of the remaining uncovered sites through dipole interactions and electron capture. Moreover, the presence of CO impurities in the anode hydrogen fuel could also significantly affect the cathode performance as a result of CO crossover from anode to cathode, probably primarily through pin-holes in the membrane [19,20].

A study concerning the CO adsorption mechanism on platinum surface is very much needed for a better understanding of the catalyst poisoning phenomena and in order to find the most reliable criteria for choosing the platinum–carbon system for real PEMFC applications. Many surface science techniques have been employed to investigate the CO adsorption process on platinum and Pt based catalysts, including low energy electron diffraction (LEED) [21–24], thermal desorption spectroscopy (TDS) [21,25], electron energy loss spectroscopy (EELS) [4,26], molecular beam scattering [27], reflection–absorption infrared spectroscopy (RAIRS) [28].

Among all the available techniques, adsorption microcalorimetry coupled to volumetry is a very powerful tool able to supply information about the number and strength distribution of the catalyst surface sites [29–31]. It can also provide a direct measurement of the heat associated to the CO adsorption on the catalyst surface (a parameter related with its surface chemistry), and the energetic distribution of the surface sites [32–34]. The heat of adsorption is perhaps the most important experimental parameter related to adsorption studies, providing a direct link to the bonding strength between adsorbed species and the surface. Therefore, the use of gas adsorption microcalorimetry is a very reliable way to obtain information which could not be extracted from another set of data alone. Table 1 lists some literature reports on the average heats of CO adsorption (at plateau or half coverage) over different platinum supported catalysts. In this table, the experimental data on powdered catalysts were collected from the vicinity of room temperature up to 130 °C. Prior to CO adsorption, the samples were reduced at 200 or 500 °C under hydrogen flow. As can be seen in Table 1, the heats of CO adsorption clearly show that CO is chemisorbed on all Pt-based catalysts (average heats of adsorption higher than 100 kJ mol^{-1}).

However, to our knowledge no data have been reported on Pt/C catalysts containing more than 15 wt.% Pt.

In the present paper, microcalorimetric measurements were used to study the adsorption of CO on different commercial carbon-supported Pt catalysts with high Pt content, which could be used in fuel cell parts such as the anode or the cathode.

In order to obtain data regarding the morphology, structure, redox features, and the influence of the carbon support on the metallic dispersion, the investigated catalysts were characterised prior to the CO adsorption measurements by using techniques such as BET, XRD, TPD-MS and TPR. Finally, the CO adsorption results were compared with those obtained from hydrogen adsorption microcalorimetry, since CO is often present in the H_2 feed under the operating conditions of a fuel cell.

Table 1
Literature data of CO adsorption over supported Pt surfaces.

Catalyst	Pt (wt.%)	Temperature of adsorption (°C)	Average heat of adsorption (kJ mol^{-1})	Reference
Pt/C (Norit RX-3)	0.22	27	115	[35]
Pt/C (Vulcan)	5.00	27	110	[36]
Pt/graphite	2.00	57	115	[37]
Pt/C	1.00	25	80	[38]
$PtSn/TiO_2$	2.00	25	105	[39]
Pt/Al_2O_3	1.88	25	120	[40]
Pt/Al_2O_3	2.00	30	135	[41]
Pt/Al_2O_3	3.00	57	130	[30,42]
Pt/Al_2O_3	5.00	50	130	[43]
Pt/SiO_2	10.00	27	135	[44]
Pt/SiO_2	1.20	130	130	[45,46]

2. Experimental

2.1. Materials

Three commercial carbon-supported platinum catalysts were used for this study, namely: Pt/C-T from Tanaka (lot 103-1341R), Pt/C-E from E-Tek (lot #E 1280702) and Pt/C-JM1 from Johnson Matthey (lot 128372001) having 24.5 wt.%, 16.8 wt.% and 16.6 wt.% of platinum, respectively. Moreover, a Pt/C-JM2 sample containing 88.3 wt.% of Pt, provided by Johnson Matthey (lot 035849-CS0323), was also tested for comparison. The catalysts were prepared by their respective proprietary manufacturing methods on C Vulcan XC72R support for Pt/C-T and Pt/C-E and on carbon black for Pt/C-JM. A typical preparation method patented by Johnson Matthey involves chemical reduction of the precursor Pt compound in aqueous slurry containing the carbon support [47] while the Pt/C-E is prepared, according to the E-Tek website, from the deposition of colloidal platinum onto the surface of activated carbon particles by oxidative decomposition of complex platinum sulphite acid (II) using hydrogen peroxide.

2.2. Characterization

The characterization of the porous texture of the carbon based materials and the determination of the specific surface area were carried out by physical adsorption of N_2 at −196 °C using a Micromeritics ASAP 2010 M apparatus. Prior to the analysis, the commercial materials were outgassed at 350 °C for 3 h. The adsorption data were analyzed using the ASAP 2010 software based on the Brunauer–Emmett–Teller (BET) isotherm and the Barrett–Joyner–Halenda (BJH) methods. The BET equation was used to calculate the apparent surface area from data obtained at P/P_0 between 0.05 and 0.22. The cross sectional area of the nitrogen molecule was assumed to be 16.2 Å. The BJH method takes into account the capillary condensation using the Kelvin equation and is useful for the determination of the pore size distribution generally for mesopores. An eventual microporosity was calculated applying the *t*-plot method. Note in this work according to IUPAC nomenclature the micropores are defined as $d < 2$ nm, mesopores $d = 2$–50 nm and macropores $d > 50$ nm. From the pore size distribution, a cumulative pore volume can be calculated. The employed technique for adsorption data analysis was valid exclusively for the micro- and mesoporous domains.

The platinum weight percentage in the catalysts was determined by inductively coupled plasma-atomic emission spectroscopy (ICP-AES). In order to dissolve them completely, the samples were treated with a mixture of $H_2SO_4 + HNO_3$ at 250–300 °C and added HCl.

X-ray diffraction spectra were recorded using a Bruker (Siemens) D5005 diffractometer (Ni-filtered CuKα radiation, λ = 1.54 Å). Measurements were performed at room temperature in the angle range of 3–80° with a step of 0.02° and a step time of 8.0 s. The platinum particle sizes were calculated from recorded XRD pattern using a whole-powder pattern fitting method (the Rietveld refinement) [48].

The surface oxygen functional groups (SOFGs) of the fresh Pt/C catalysts were determined by temperature-programmed desorption using a coupled TG-DSC equipment linked to a MS in a continuous helium flow (30 mL min^{-1}) with heating from room temperature to 700 °C at a rate of 5 °C min^{-1}. During this temperature increase, the mass spectrometer was set at $m/e = 28$, 44 and 18 for CO, CO_2 and H_2O, respectively. The experimental

conditions selected for the TPD run ensure that secondary reactions between desorbed CO and surface bound oxygen complexes are kept to a minimum. Thus, a low heating rate (such as 5 °C min^{-1}) helps to maintain a low intrapore concentration of CO and a sufficiently high flow rate (30 mL min^{-1}) works in the same direction [49].

Conventional temperature-programmed reduction experiments (TPR) were performed on the three commercial samples using a TPD/R/O-1100 instrument (ThermoFisher). The gas used in TPR was a mixture of 4.98% (v/v) H_2 in Ar, and the oxidizing gas was a mixture of O_2/He (0.998% O_2). The flow rate of the TPR gas was 20 mL min^{-1} (STP) and a heating rate of 10 °C min^{-1} was used. The catalyst samples weighed 0.03–0.04 g. The procedure for a TPR measurement consisted in the following steps: (1) The fresh catalyst sample was calcined in O_2/He mixture for 1 h at 400 °C, cooled to 30 °C in the same gas mixture, switched from O_2/He to Ar and maintained in Ar atmosphere for 30 min at 30 °C, and then switched from pure Ar to the H_2/Ar mixture. (2) After returning to the base line, TPR was carried out in the H_2/Ar mixture from 30 °C up to 950 °C. The H_2 consumption was detected by a thermal conductivity detector (TCD) which was quantitatively calibrated by carrying out the reduction of pure CuO and assuming that it is completely reduced to metallic copper. Therefore, it was possible to determine the hydrogen consumptions from the TPR peak areas.

The CO and hydrogen adsorptions were studied by adsorption microcalorimetry measurements. The adsorption experiments were performed at 30 °C in a heat-flow microcalorimeter (Tian-Calvet type, C80 from Setaram) linked to a conventional volumetric apparatus and equipped with a Barocel capacitance manometer (Datametrics) for pressure measurements. The activation procedure and the CO adsorption were designed in such a way as to reproduce as closely as possible the adsorption of CO in real PEMFCs. The activation process was performed at room temperature (RT) (about 25 °C) in the calorimetric quartz cell. The catalysts, fresh samples (around 0.08 g), were pretreated under vacuum for 2 h at RT, after which 200 Torr of hydrogen were admitted into the system and left to react overnight. Before CO adsorption, the catalysts were outgasssed also at RT for 2 h in order to remove excess and physisorbed hydrogen. CO was further adsorbed over a surface previously covered with hydrogen. The situation is similar to that in fuel cells, where CO comes at the anode surface as an impurity in the hydrogen flow. The differential heats of adsorption were measured as a function of coverage by repeatedly sending small doses of CO over the catalyst until an equilibrium pressure of about 0.5 Torr was reached [50,51]. The sample was then outgassed for 30 min at the same temperature and a second adsorption was performed (still at 30 °C) until an equilibrium pressure of about 0.2 Torr was attained, in order to calculate the amount of irreversibly chemisorbed carbon monoxide at this pressure. The difference between the amounts of gas adsorbed at 0.2 Torr during the two adsorption runs corresponds to the number of strong adsorption sites. The dispersion of the metal was determined concomitantly to the adsorbed volume by means of CO adsorption. The same procedure was also used for hydrogen adsorption measurements.

In this work, four successive CO adsorption/desorption/readsorption cycles were performed on the same batch of sample for each catalyst. Blyholder and Sheets [52] found that exposure to air for 12 h at RT eliminated the IR bands assigned to CO adsorbed on Pt sites. Therefore, between two successive CO adsorption cycles, the catalysts were kept in the calorimetric cell under air at room temperature and again reactivated as described in Table 2. In addition, it is worth noticing that the pretreatment was performed at room temperature in order to be as close as possible to the operating conditions of real fuel cells.

Table 2
Experimental conditions used to perform CO adsorption/desorption/readsorption cycles[a] at 30 °C with the adsorption microcalorimetry technique.

Run number	I	II	III	IV
Pretreatment at 25 °C (in h)				
In air	–	24	72	24
In vacuum	2	2	2	2
In hydrogen (200 Torr)	12	12	12	12
In vacuum	2	2	2	2

[a] CO adsorption was performed until an equilibrium pressure of 0.5 Torr was reached, followed by desorption under vacuum until the equilibrium was attained. A second CO adsorption was then performed after pumping at 30 °C until an equilibrium pressure of 0.2 Torr was reached.

3. Results and discussion

3.1. Physico-chemical characterization

Nitrogen adsorption isotherms were measured at −196 °C for the studied catalysts and the results are presented in Fig. 1 and Table 3. Table 3 also presents the amounts and the crystallite sizes of platinum in the samples as determined by the ICP-AES and XRD methods, respectively.

Pt/C-T, Pt/C-E and Pt/C-JM1 present adsorption/desorption isotherms which belong to type IV in the IUPAC classification [53]. The high nitrogen uptake at P/P_0 approaching 1 indicates that the catalysts present large mesopores besides a small microporosity.

As listed in Table 3, similar total pore volumes were measured for all studied catalysts. Pt/C-JM2 presents a much smaller surface area, around 15 m^2 g^{-1}, and consequently no other parameters were

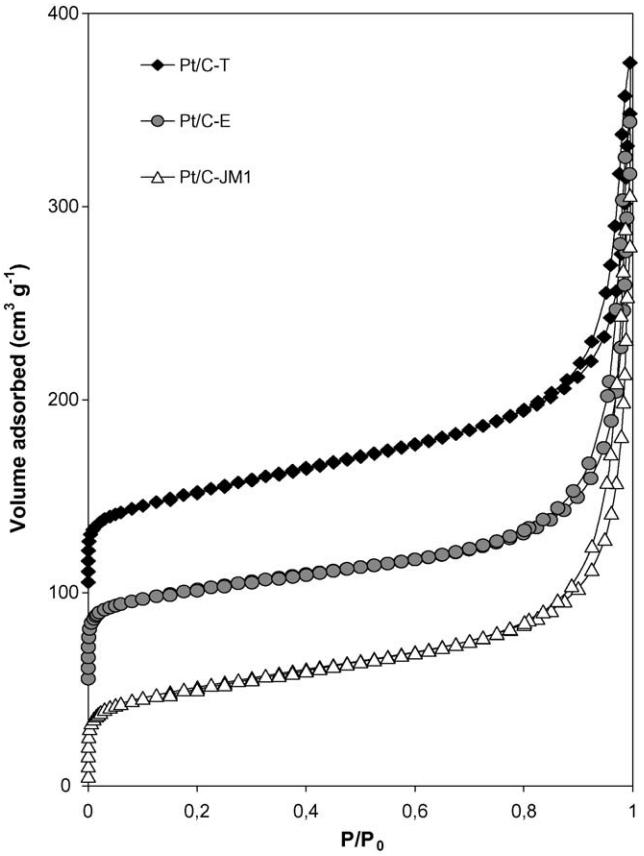

Fig. 1. Nitrogen adsorption isotherms at −196 °C for Pt/C-T, Pt/C-E and Pt/C-JM1 catalysts.

Table 3
Physico-chemical properties of Pt/C catalysts.

Catalyst	Loaded Pt (wt.%)	XRD data	Surface area			Pore volume		
		Crystallite size (nm)	S_{BET} ($m^2 g^{-1}$)	S_{BJH} ($m^2 g^{-1}$)	S_{micro} ($m^2 g^{-1}$)	V_{single} ($cm^3 g^{-1}$)	V_{BJH} ($cm^3 g^{-1}$)	V_{micro} ($cm^3 g^{-1}$)
Pt/C-T	24.5	1.5	186.1	132.4	28.8	0.27	0.36	0.01
Pt/C-E	16.8	1.5	179.2	88.3	59.7	0.27	0.37	0.03
Pt/C-JM1	16.6	1.9	181.9	100.3	60.0	0.28	0.39	0.03
Pt/C-JM2	88.3	5.6	15.2	nd	nd	nd	nd	nd

S_{BET} is the surface area calculated by the BET method; S_{BJH} and V_{BJH} are the cumulative adsorption surface area and pore volume respectively ($1.7 <$ pore diameter < 300 nm) calculated by the BJH method; S_{micro} and V_{micro} are respectively the surface area and pore volume in the micropore range (pore diameter < 2 nm) calculated by the deBoer's *t*-plot method; V_{single} is the single point total pore volume (pore diameter < 100 nm).

determined for this powder. As can be seen, the commonly used BET method gave surface area values larger than the BJH approach (e.g. 186.1 $m^2 g^{-1}$ vs. 132.4 $m^2 g^{-1}$ for Pt/C-T), which is expected since BET refers to the total surface area (including micropores), while BJH is typically valid for mesopores. DeBoer's *t*-plot micropore analysis was performed in order to check the microporosity of the Pt/C catalysts, knowing that the presence of micropores (diameter < 2 nm) leads to a poor utilization of the catalysts in the PEM fuel cell assembly, as the catalyst particles present in the micropores are often not accessible to the fuel [54,55]. As can be seen in Table 3, microporosity is more significant in the Pt/C-E and Pt/C-JM1 samples, while mesoporosity dominates in the Pt/C-T catalyst. The BET surface areas of the Pt/C-T and Pt/C-E catalysts are smaller than that of the C Vulcan XC72R support ($S_{BET} = 225$ $m^2 g^{-1}$, determined in the same experimental conditions as used for the platinum based catalysts). Moreover, comparison with data found in the literature concerning the carbon Vulcan XC72R support ($S_{BET} = 223$ $m^2 g^{-1}$, $V_{micro} = 0.136$ $cm^3 g^{-1}$; BJH cumulative surface area = 134 $m^2 g^{-1}$) [47] leads to the conclusion that the micropore volume was also reduced by the presence of the active phase, thus indicating that Pt nanoparticles block some of the micropores in the support. This fact is more visible for Pt/C-T ($V_{micro} = 0.01$ $cm^3 g^{-1}$). For Pt/C-T, the BJH area is only slightly lower than that of the support itself since the mesopores are less obstructed by the platinum particles. This fact is important in the catalyst layer of PEM fuel cell, from the point of view of Nafion membrane penetration. Two types of pores were observed for the three catalysts: large mesopores and a small microporosity. The mesopore diameters were obtained from the adsorption branch of the isotherm using the corrected form of the Kelvin equation by means of the Barrett–Joyner–Halenda method and were 10.7, 16.7 and 15.7 nm for Pt/C-T, Pt/C-E and Pt/C-JM1, respectively. To characterize the micropore size distribution, the Horvath-Kavazoe method was used; the diameters obtained were 1.2, 2.0 and 1.1 nm for Pt/C-T, Pt/C-E and Pt/C-JM1, respectively.

The crystalline structure of the catalysts was determined by the powder X-ray diffraction technique and the results are presented in Fig. 2 and Table 3. The five major diffraction peaks of platinum for a Pt/C catalyst are at $2\theta = 39.7°$ (1 1 1), 46.2° (2 0 0), 67.4° (2 2 0), 81.2° (3 1 1), and 87.3° (2 2 2) [56]. With the exception of the first broad peak around 25° (less evident for Pt/C-JM2 with only around 10 wt.% C) associated with the (0 0 2) diffraction peak of the hexagonal structure of the carbon support, the Pt/C catalysts exhibited a typical Pt face-centered cubic (fcc) crystal structure. The most intense peak at $2\theta = 39.8°$ is related to the Pt (1 1 1) plane and is clearly recognizable in all patterns. The other main diffraction peaks of Pt/C samples centered at $2\theta = 46.5°$ and 67.8° should be ascribed to Pt (2 0 0) and Pt (2 2 0) crystal surfaces, respectively. Except for the peaks already mentioned above, there are no other distinct reflection peaks in the spectra.

The diffraction peaks of the powders provided by Johnson Matthey are higher and narrower than those of samples Pt/C-T and Pt/C-E, which indicates that the Pt/C-JM1 and Pt/C-JM2 samples display larger metallic particle sizes than the two other catalysts. Indeed, according to X-ray analysis (Rietveld method [48]), the average crystallite sizes of the Pt/C powders are increasing in the following order: Pt/C-T = Pt/C-E < Pt/C-JM1 < Pt/C-JM2 (see Table 3).

It is well known that the metallic dispersion on carbon supports is controlled by (i) the porous structure of the activated carbons, (ii) the oxygen groups present on their surface, and (iii) specific interactions of metal precursors with surface defects or graphite edges [57]. The TPD-MS technique was used in this study to determine the surface chemistry of the Pt/C catalysts (Fig. 3A and B). Upon heating, the decomposition of oxygen-bearing surface groups giving rise to CO and CO_2 at different temperatures is well proved in the literature [49,57,58]. Although there are different proposals for the assignment of the peaks to specific surface groups, general trends can be established and they are well accepted in the literature; temperature differences between the peaks have been reported to be as high as 50–100 °C [49]. Thus, the low temperature CO_2 peak results from decomposition of carboxylic acids, while the high temperature CO_2 peak can be assigned to the presence of lactones. The decomposition of carboxylic anhydrides can be assigned to both CO and CO_2 peaks and decomposition of phenols, ethers, carbonyls and quinines to CO peaks at higher temperatures.

The application of the TPD technique to the four Pt/C catalysts showed differences in surface chemistry among the investigated samples. The TPD-MS curves of CO_2 evolved are shown in Fig. 3A. The obtained CO_2 spectra for the investigated samples are in agreement with those obtained in the literature (wide peak with several shoulders) [58]. The CO_2 profiles for Pt/C-T and Pt/C-E catalysts are almost similar, presenting quite distinct peaks which can be tentatively assigned to different functional groups by comparison with the available literature data [49,58,59]. CO_2 evolution with temperature for Pt/C-T sample

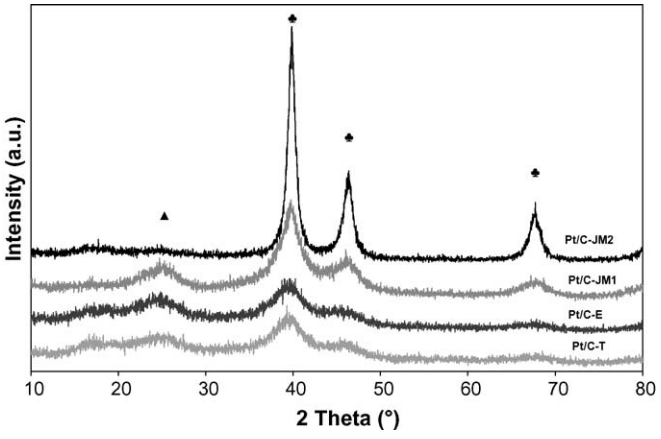

Fig. 2. X-ray diffraction patterns of the Pt/C catalysts: (▲) diffraction line of C; (♣) diffraction lines of Pt.

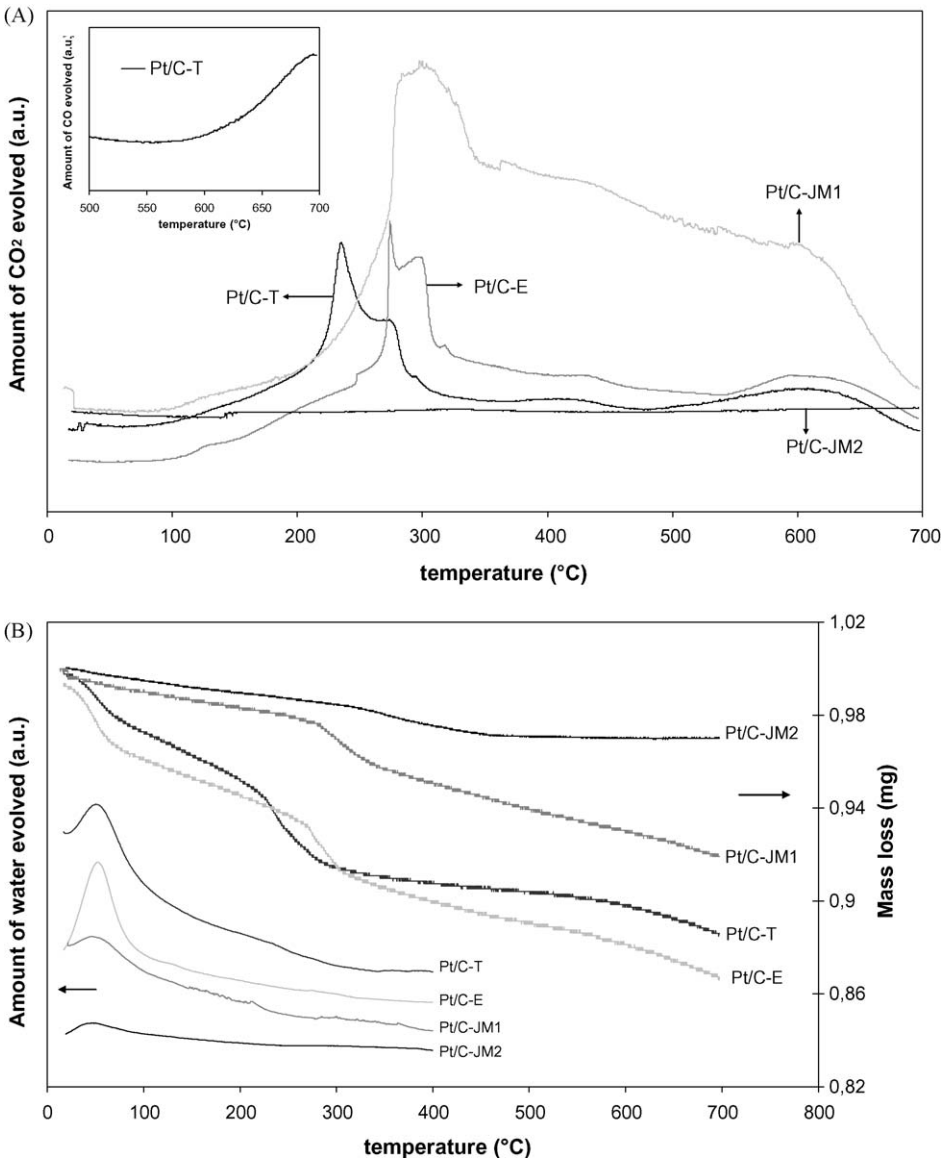

Fig. 3. (A) CO_2 TPD-MS profiles of the Pt/C-E, Pt/C-T and Pt/C-JM catalysts (at the upper side is shown the corresponding CO-TPD profile for Pt/C-T powder); (B) the corresponding TG experiments and H_2O-TPD profiles for Pt/C catalysts.

presents a maximum at 237 °C with shoulders at 270, 297, 416 and 604 °C, while for Pt/C-E the maximum was observed at 272 °C with shoulders at 251, 300, 320, 435 and 608 °C. CO_2 evolution at low temperature could be attributed to the presence of SOFGs (surface oxygen functional groups) of the carboxylic acid functions, while the small CO_2 peaks at higher temperature may result from anhydrides and lactones. No CO evolution was detected from the catalysts provided by Johnson Matthey (Pt/C-JM1 and Pt/C-JM2), while the CO evolution in the TPD-MS spectra for the two other studied samples started at about 600 °C as can be seen in the insert of Fig. 3A. Due to the similarity of the results obtained for the Pt/C-T and Pt/C-E catalysts, only the CO profile of Pt/C-T is presented. The presence of CO above 600 °C may originate from phenols, ethers, and carbonyls/quinines. For Pt/C-JM1, the CO_2 profile (Fig. 3A) presents a maximum at 300 °C and shoulders at 287, 441 and 598 °C. This sample is richer in oxygen bearing surface groups compared to the Pt/C-T and Pt/C-E catalysts. The spectrum corresponding to Pt/C-JM2 presents a very low amount of surface oxygen complexes, not appreciable at the scale used. The low amount of CO_2 detected for this catalyst is due to carboxylic acids, lactones and anhydrides. These SOFGs constitute about 8.75, 7.50 and 6.75 wt.% of the total mass of Pt/C-JM1, Pt/C-E and Pt/C-T, respectively, as determined by TG experiments (mass loss (mg) vs. temperature (°C) plots shown in Fig. 3B). As can be seen, the first part of the TG curves is due to water removal, as detected by TPD-MS (see the bottom part of Fig. 3B), and was not considered in the calculations. For Pt/C-JM2, a very small amount of water was detected by TPD-MS and the mass loss of around 2 wt.% observed by TG was considered to come from the decomposition of SOFGs. CO_2 evolution from the C Vulcan XC72R support (not presented in Fig. 3A) was very small and could correspond to oxygen complexes formed upon air exposure at room temperature during its storage.

Fig. 4 reports the temperature-programmed reduction profiles obtained for the carbon-supported Pt catalysts. For comparison the TPR profile of C Vulcan XC72R support is also presented. The carbon support presents one hydrogen consumption zone at temperatures between 650 and 950 °C, which can be explained both by adsorption on free carbon sites created upon decomposition of oxygen bearing surface groups anchored on them (e.g. desorption of COOH, C=O, or C–O–C groups), and additionally by some carbon gasification. As proved by TPD measurements, thermal treatment removes oxygen in the form of CO_2 (pre-

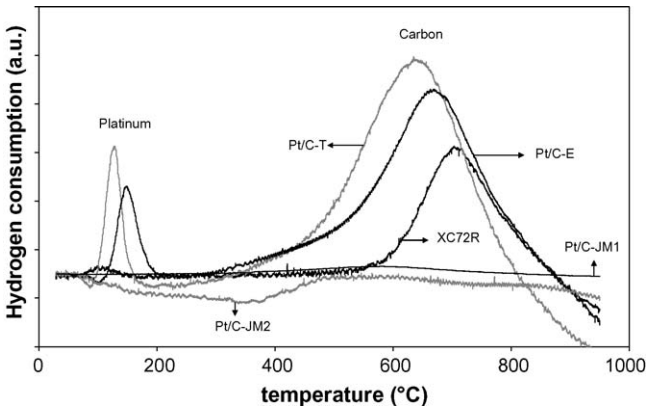

Fig. 4. Temperature-programmed reduction profiles for Pt/C catalysts and XC72R support from Vulcan.

dominantly at lower temperatures) and CO (predominantly at higher temperatures), leaving unsaturated carbon atoms at the edges. Hydrogen treatment removes the least saturated carbon atoms from the edges (probably as methane) and also forms stable C–H bonds with the carbon active sites [60].

No hydrogen consumption was observed for Pt/C-JM2 and Pt/C-JM1 samples at low temperatures. These catalysts show a nearly flat profile; it seems that (i) if PtO_x species were formed during pretreatment under oxygen, then they could have been reduced to metallic Pt at lower temperature during the flushing in inert gas (see Experimental) or (ii) the two catalysts are very stable in our experimental conditions. For Pt/C-JM1, only a broad reduction peak at higher temperature was observed, however this peak does not seem significant when compared with the results obtained for Pt/C-T and Pt/C-E. The E-Tek and Tanaka catalysts present a first hydrogen consumption peak at 130 and 151 °C for Pt/C-T and Pt/C-E, respectively. The difference observed in these temperature maxima can be attributed (i) to stronger platinum-support bonds on Pt/C-E catalyst; or (ii), as Ostgard et al. [61] found in their study, to the smaller loading of Pt on the E-Tek catalyst compared with the Tanaka sample, which induces a shift of the reduction temperature to higher values. It has to be pointed out that the data in the literature concerning oxidized Pt species are not fully in agreement. For example, for a Pt/Al_2O_3 catalyst, Lieske et al. [62] found that highly dispersed Pt is completely oxidized to the valence state +4 by oxygen treatment between 400 and 600 °C, the Pt^{4+} species being reduced at around 250 °C. However, Ostgard et al. [61] found that the valence of the Pt ions resulting from oxidation at temperatures ranging from 25 to 400 °C is only +2, while at 500 °C, Pt^{4+} ions can be formed. In this work, the integration of the low temperature TPR peaks obtained for Pt/C-E and Pt/C-T catalysts revealed a Pt valence of +2. The peak corresponding to the reduction of Pt (II) species to metallic state is more intense for Pt/C-T due to the higher amount of Pt on this catalyst and consequently the higher amount of H_2 needed for its complete reduction. According to the measurement of the consumed hydrogen amount corresponding to this peak, a H_2/Pt molar ratio close to one was found for both catalysts.

The second hydrogen consumption peak observed in Fig. 4, which appears at high temperature (maximum above 600 °C) for both Pt/C-T and Pt/C-E catalysts and to a lower extent for Pt/C-JM1, is similar to that found in the TPR profile of the Vulcan XC72R support. Hence, this H_2 consumption zone would be related to the decomposition of weak functional groups of the support, which leads to the formation of new unsaturated reactive surface sites able to consume hydrogen and additionally to form methane by carbon gasification, a reaction which is known to be catalysed by the supported platinum [35,63,64]. Radovic and co-workers [60,65] found that when Pt/C is treated under H_2 at high temperature the most significant process occurring is the hydrogasification of the most reactive carbon atoms. Platinum particles dissociate hydrogen molecules, creating hydrogen atoms that "spill over" to the carbon surface, both via surface and gas-phase diffusion, hydrogasifying the most reactive surface carbon atoms. That is, the hydrogen atoms remove (probably in the form of methane) carbon atoms that are left in a highly unsaturated state due to the prior thermal removal of neighboring carbon atoms (evolved as CO_2 or CO).

Table 4
CO adsorbed amounts ($\mu mol_{CO}\,\mu mol_{Pt}^{-1}$), dispersion ($D$, %), mean particles size (d, nm) and average adsorption heats determined from CO adsorption microcalorimetry at 30 °C for commercial Pt/C catalysts.

Sample	D (%)	d (nm)	No. of cycle adsorption	Q_{diff}[a] ($kJ\,mol^{-1}$)	CO uptake	
					n_{total}[b] ($\mu mol\,g_{Pt}^{-1}$)	n_{irrev}[c] ($\mu mol\,g_{Pt}^{-1}$)
Pt/C-T	27	4	I	135	1331	1232
			II	146	1223	1142
			III	150	1109	1032
			IV	151	1164	1082
Pt/C-E	27	4	I	155	1308	1230
			II	155	1233	1165
			III	149	1202	1124
			IV	146	1180	1089
Pt/C-JM1	32	3	I	148	1413	1253
			II	146	1324	1175
			III	146	1380	1232
			IV	147	1386	1245
Pt/C-JM2	–	–	I	158	191	177
			II	177	185	173
			III	167	148	136
			IV	162	133	122

[a] Differential heats calculated as average of the plateau values.
[b] Amount of CO adsorbed under an equilibrium pressure of 0.2 Torr.
[c] Amount of irreversibly chemisorbed CO.

3.2. Adsorption microcalorimetry study

Table 4 shows the CO adsorption uptakes, platinum dispersions and mean particle size values as determined from the microcalorimetry measurements for all studied catalysts. The average CO adsorption heats (Q_{diff}) are also shown in order to enable a comparison among samples and with the literature data (Table 1). The average heat values may be taken as a criterion to compare the adsorption strengths of the main exposed sites, knowing that the heats of adsorption correspond to an average over all adsorbed surface species. Consequently, the average heat of adsorption has been considered more relevant for this study and not the initial or integral heats, which are less representative of the global adsorption site strength.

The metal dispersion (D) was calculated by taking into account the total platinum loading and the total CO uptake at the monolayer considered to be attained when the evolved heat falls to the physisorption field, and assuming a Pt:CO = 1:1 stoichiometry [42,43,66]. The mean crystallite sizes were calculated from the dispersion values, assuming spherical metal particles, using the equation d (nm) = 1.08/D [66].

From the data in Table 4 it can be seen that for similar platinum content (Pt/C-E and Pt/C-JM1 with about 16 wt.% Pt), the dispersion and mean particle size seem to depend on the sample's history, given that for example the surface chemistry of the support (i.e. the porosity and the amount of oxygen bearing surface groups of the carbon material) plays a role in controlling the final

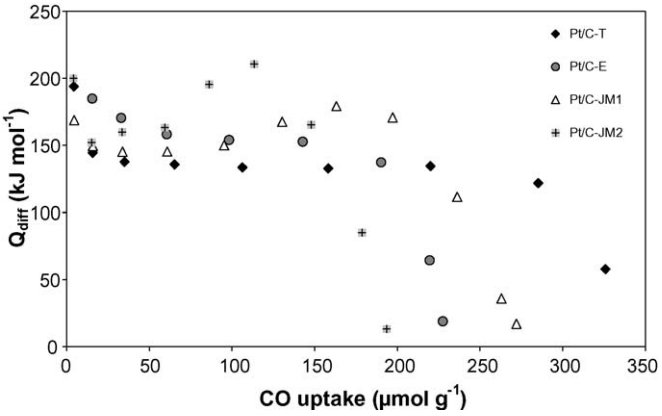

Fig. 5. Differential heats of CO adsorption at 30 °C as a function of surface coverage for Pt/C-T, Pt/C-E, Pt/C-JM1 and Pt/C-JM2 catalysts.

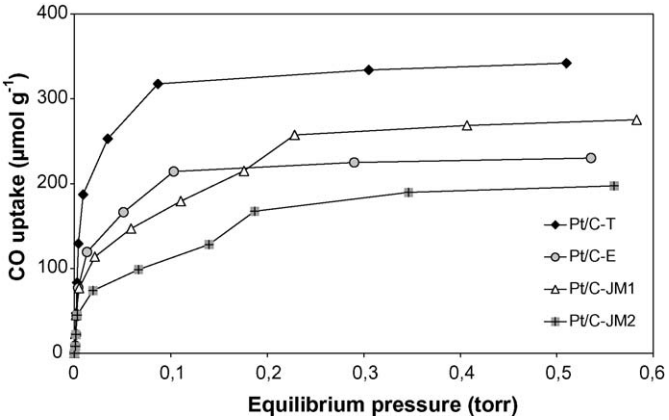

Fig. 6. Volumetric calorimetric isotherms of CO adsorption on Pt/C catalysts at 30 °C.

metal dispersion. The effect of the surface chemistry of the carbon support can be observed considering Pt/C-E and Pt/C-T, since they display similar dispersion data despite different platinum loadings.

The mean particle sizes obtained from microcalorimetric data (CO chemisorption) are higher than those obtained from XRD data (Rietvelt refinement) (see Tables 3 and 4). These results can be explained by the smaller dispersion obtained when CO adsorption is used instead of hydrogen for such measurements. Indeed, Prado-Burguete et al. [66] and Rodriguez-Reinoso et al. [67] found that the dispersions calculated from CO chemisorption are, in general terms, smaller than those determined from H_2 chemisorption due to a greater contribution of bridge-bonded CO on small particles.

The average values of CO adsorption heats (first cycle) for the Pt/C samples are 135, 155, 148 and 158 kJ mol^{-1} for Pt/C-T, Pt/C-E, Pt/C-JM1 and Pt/C-JM2, respectively. Except for Pt/C-T, these values are slightly higher than those reported in Table 1.

Fig. 5 represents the variations of the differential CO adsorption heats with carbon monoxide coverage. A comparison of the studied catalysts shows some differences concerning the surface site distributions. In this sense, Pt/C-JM2 shows a more heterogeneous surface site distribution as no plateau (coverage zone for which the adsorption heat is nearly constant) appears in the variation of differential heats vs. CO coverage. After a sharp decrease off the initial heats, by about 50 kJ mol^{-1}, a smooth increase of the heats can be observed with increasing coverage, followed by another sharp decrease at CO uptakes higher than 120 μmol g^{-1}. This behaviour was not expected, and may be explained by interactions between CO molecules with possible carbonyl formation and/or by the displacement of some remaining hydrogen. This last hypothesis is more convincing and confirmed by the shape of the adsorption isotherms (Fig. 6). To a smaller extent, a similar variation of the CO adsorption heats with coverage can be also observed for Pt/C-JM1. This catalyst exhibits a short plateau at about 150 kJ mol^{-1} in the low CO coverage domain (up to 100 μmol CO g^{-1} catalyst), followed by a slight increase of adsorption heats up to 180 kJ mol^{-1} and then a sudden drop of Q_{diff} to 17 kJ mol^{-1}. In systems in which kinetics and not equilibrium essentially control the adsorption process, Gow and Phillips [68] have shown that observed differential heats of adsorption will not necessarily be monotonically decreasing. Fluctuating or increasing heats of adsorption can be observed if kinetics dominates the adsorption/rearrangement process.

For sample Pt/C-E, a continuous and slow decay of the differential heats (from 200 kJ mol^{-1} to around 160 kJ mol^{-1}) is observed until a CO uptake of 60 μmol g^{-1} catalyst. A further increase in the CO coverage produces the occurrence of a plateau (around 155 kJ mol^{-1}) followed by a sharp fall in the heats at monolayer formation. Pt/C-T appears to be rather simple and characteristic of a clean, hydrogen- or oxygen-free platinum surface. Its variation of differential heats shows a plateau at ~135 kJ mol^{-1} for a wide range of CO coverage (up to 220 μmol g^{-1} catalyst), suggesting that the majority of the sites present at the surface of this catalyst have a very similar geometry and energy of interaction with the CO molecules. The drop in the differential heats at higher coverage is indicative of saturation of the accessible platinum metallic surface sites. The high initial heats of adsorption can be attributed to a small amount of CO adsorbed on low coordinated platinum atoms, at corners or edges [30,39].

In fact, as may be inferred from spectroscopic data [69], two different types of adsorption sites can be found on platinum, respectively identified as linear (around 2076 cm^{-1}) and bridged sites (1857 cm^{-1}). The microcalorimetry results, with rather similar adsorption heat values in a large domain, can suggest that the main adsorbed species, over all Pt/C catalysts, are linear (Pt-CO). However, the presence of SOFGs on the support could modify the strength of the Pt-CO bonds. In fact, the differences observed at low CO coverage values could be due to the contribution of the support to the surface properties of the catalysts. It is known that electron-donating supports such as graphite produce an enrichment of the electron density of metal atoms interacting with them [70], inducing changes in the chemisorption properties of the metal particles; these facts have been evidenced by CO adsorption microcalorimetry [71].

As already mentioned, the particular features observed in the calorimetric curves are even more apparent in the volumetric isotherms presented in Fig. 6. The Pt/C-T and Pt/C-E samples present similar characteristics, with a CO adsorption directly related to the amount of Pt loading. The amounts adsorbed up to the knee of the isotherm that can be approximately identified as the completion of the metal surface coverage were found to be 219, 322, 253 and 177 (with an experimental uncertainty of ±5) μmol g^{-1} catalyst for Pt/C-E, Pt/C-T, Pt/C-JM1 and Pt/C-JM2, respectively. The sudden increases of CO uptake around 0.2 Torr for Pt/C-JM samples correspond to the bell shape in the calorimetric curves and can be attributed to a displacement of remaining hydrogen on the surface which can occur only when a certain CO residual pressure is attained.

The irreversibly chemisorbed amount of CO (n_{irrev}) can also be measured from the calorimetric studies as described in the experimental section. Obviously, this volume corresponds to the total amount held by the strong chemisorption sites at the adsorption temperature over the catalysts. As can be deduced from Table 4 which summarizes n_{irrev}, n_{total} as well as the average heats

of CO adsorption, CO is almost completely irreversibly adsorbed on the surface of the Pt/C catalysts (i.e. 94, 93, 93 and 89% for Pt/C-E, Pt/C-T, Pt/C-JM1 and Pt/C-JM2, respectively). As another measure of the average strength of the CO adsorption sites, the ratio $Q_{int,total}/n_{total}$ was also calculated, $Q_{int,total}$ being the integral heat of adsorption corresponding to n_{total}. This quantity decreases in the following order: Pt/C-JM2 (161 kJ mol^{-1}) > Pt/C-E (147 kJ mol^{-1}) > Pt/C-JM1 (144 kJ mol^{-1}) > Pt/C-T (129 kJ mol^{-1}) and is quite comparable to the average values of differential heats reported in Table 4.

In contrast to other techniques for studying adsorption, heat-flow calorimetry yields both differential kinetic and thermodynamic information. The kinetics of heat release during adsorption can be monitored by changes in the thermokinetic parameter τ. The calorimetric signal decreases exponentially with the adsorption time after the maximum of each adsorption peak. This can be expressed in the form $D(t) = D_m \exp(-t/\tau)$, where $D(t)$ and D_m are the deviation at time t and the maximum deviation of the calorimetric signal, respectively. The thermokinetic parameter τ in this expression can thus be computed as the inverse of the slope of the logarithm of the evolved heat curve during the return to equilibrium, and depends mainly on the accessibility of the adsorption sites in the samples. The variation of the thermokinetic parameter with the amount of adsorbed CO is shown in Fig. 7 for the various samples. For sample Pt/C-E, the thermokinetic parameter at first increases to reach a maximum and then decreases. To some extent the same trend was observed for Pt/C-JM1 catalyst, but with shorter times for the heat evolution. It is well known that the pore architecture (e.g. pore volume and pore size distribution) of a heterogeneous catalytic material controls gas transport phenomena. A comparison with Table 3 shows the influence of microporosity on the variation of τ. The higher the microporosity of the catalyst, the higher the thermokinetic parameter becomes. The smallest values and variations of the thermokinetic parameter were observed for Pt/C-T and can be attributed to a high mobility of the CO molecules on the catalytic surface. Indeed, the diffusion was not limited by movement of CO through micropores. More mesoporosity facilitates the creation of larger paths for diffusion, leading to an increased accessibility of CO molecules to the adsorption sites in the samples. Sample Pt/C-JM2 presents a variation of the thermokinetic parameter vs. coverage with a maximum corresponding to the measured n_{irrev} value.

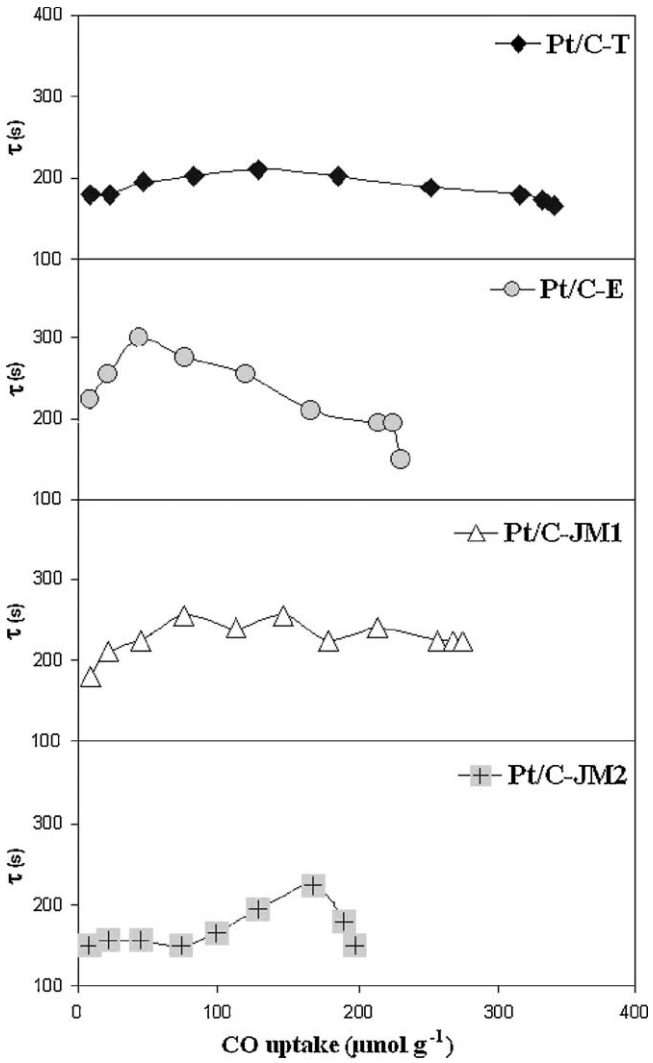

Fig. 7. Thermokinetic parameter, τ, vs. CO uptake for studied Pt/C catalysts.

The aging of the three catalysts under successive cycles in different atmospheres (pretreatment under air, reduction under static H_2 atmosphere and adsorption of CO) was determined by performing four series of microcalorimetric measurements at 30 °C for each sample, on the same batch of powder (see Experimental).

The repeated exposure of the samples to air and subsequent reduction in static hydrogen atmosphere, at room temperature, induced some differences in the CO adsorption properties of the Pt/C catalysts. The CO adsorption capacity decreased after each new microcalorimetric measurement as can be seen in Table 4 (CO uptake), which could be explained by the partial surface coverage of platinum particles by chemisorbed CO species. It seems that the catalyst is partly poisoned and the exposure in air followed by the reduction in a static hydrogen atmosphere at room temperature is not sufficient to remove all CO species adsorbed on the sample surface.

Fig. 8A–D shows the CO differential heats versus coverage plots corresponding to the different cycles on each catalyst. With the exception of sample Pt/C-JM1, whose curves for each CO adsorption run are almost superimposed, differences can be observed in the adsorptive properties of the other Pt/C catalysts. For sample Pt/C-T (Fig. 8A), the initial heats of adsorption lie in the range 167–209 kJ mol^{-1} for the four CO adsorption cycles, all decreasing sharply to ~145 kJ mol^{-1} with increasing coverage. Differences appear in the region of intermediate CO uptake, where the plateau observed for the first adsorption over a wide range of coverage disappears and a slight increase of Q_{diff} can be observed above a CO coverage of 100 μmol g^{-1} catalyst. This behaviour can be attributed to CO-CO or H-CO interactions and appears for CO coverages in the range of 100–250 μmol g^{-1} catalyst. This phenomenon was already observed for the fresh Pt/C-JM samples (see Fig. 5) and argues in favour of the displacement of remaining hydrogen on the catalyst surface. In the region of high CO uptake, a fast decrease of Q_{diff} can be observed, indicating the saturation of the adsorption surface sites. Except for CO adsorption on the fresh catalyst (the first adsorption), a reproducible site energy distribution was observed in the next three successive adsorption cycles.

The profiles of the differential heats of CO adsorption as a function of CO uptake at 30 °C were more similar for the four microcalorimetric cycles performed on Pt/C-E, despite the initial heats of adsorption decreasing with each new CO adsorption run (Fig. 8B). It has to be pointed out that, even if to a lower extent compared to Pt/C-T, a bell-shaped curve of Q_{diff} with CO uptake was observed at coverages higher than 100 μmol g^{-1} catalyst until the fall of heat values into the physisorption domain. For the Pt/C-JM1 catalyst (Fig. 8C), it seems that the pretreatment under air and then under hydrogen is the most efficient since no changes in the adsorptive properties of this sample were observed at the end of

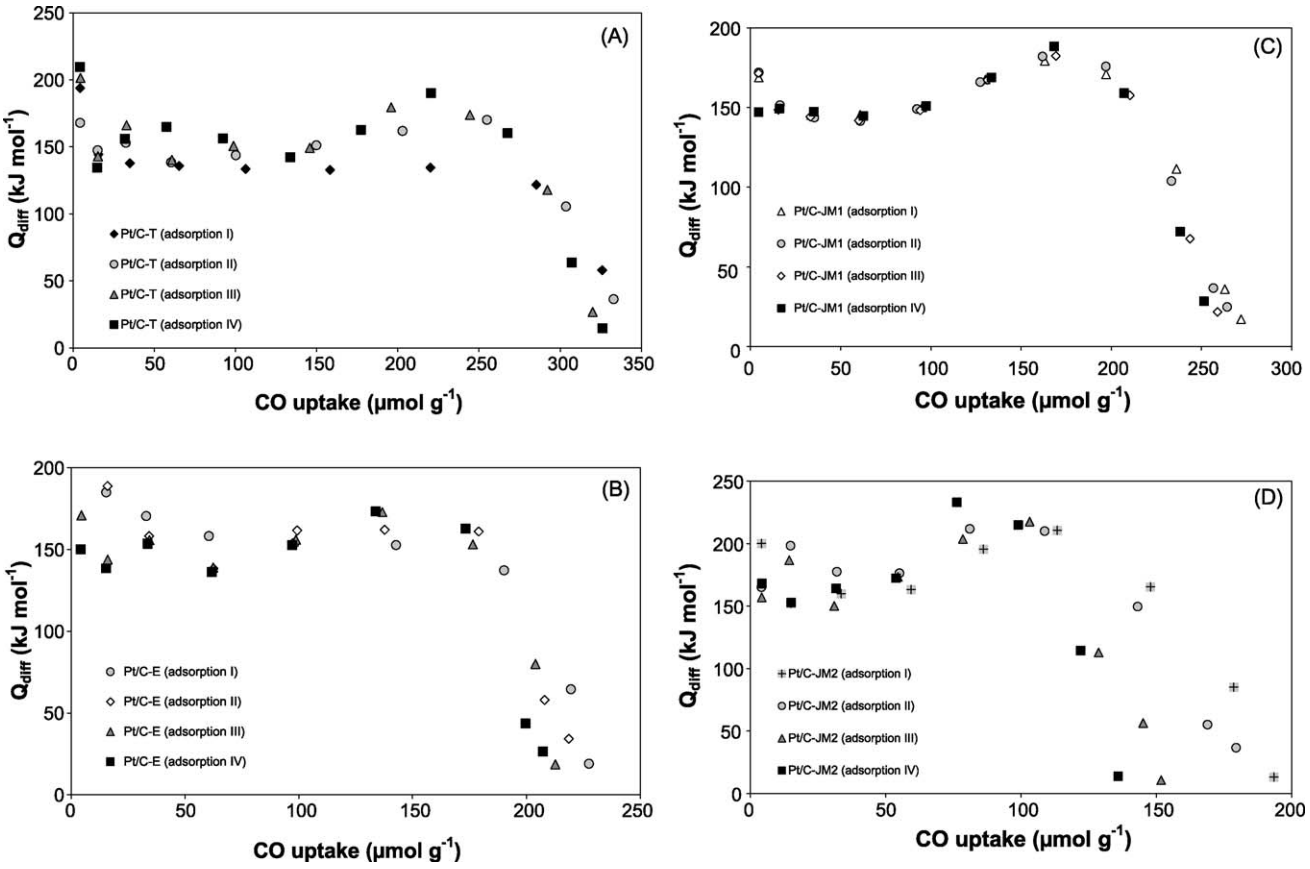

Fig. 8. Differential heats of the four CO adsorption cycles performed at 30 °C as a function of surface coverage for the tested catalyst.

the experiments. This behaviour suggests that the platinum particle morphology, structure and adsorbed CO species are restored or remain unchanged, independently of the repeated exposure to air/H_2/CO. For the Pt/C-JM2 powder (Fig. 8D), the bell shape is more and more pronounced with successive cycles. Differences appear in the total amount of CO adsorbed after each cycle, which decreases considerably at the end of the experiments. For the studied catalysts, 2, 10, 13 and 30% of accessible Pt sites were irreversibly poisoned by CO for Pt/C-JM1, Pt/C-E, Pt/C-T and Pt/C-JM2, respectively. Indeed, the decrease in CO adsorption capacity, which means a decrease in the number of adsorption sites, can be attributed to an irreversible poisoning of the surface.

It has to be pointed out that the initial CO adsorption heat values obtained for all studied catalysts are higher than those found in the literature for CO adsorption over supported platinum catalysts (115 kJ mol^{-1} for a polycrystalline Pt/C catalyst [35,36], 107 kJ mol^{-1} for Pt/C [38] or 140 kJ mol^{-1} for Pt/SiO_2 [45]). It is well known that the heat of adsorption increases with decreasing average coordination number of the surface metal atoms, due to preferential adsorption on low coordination sites such as edges and corners [36,37,42]. Thus, this finding would indicate that a certain amount of highly unsaturated platinum atoms and open faces is present in the catalysts investigated in the present study. Also, it has to be pointed out that the amount of supported platinum in the samples described in the literature was much smaller than in this study and that the catalysts were reduced at temperatures higher than RT [35,36,38–40,44,45]. On the other hand, the high initial adsorption heats observed in this study can be due to interaction of CO with some remaining oxygen species on the catalyst surface. Wartnaby et al. [72] have used calorimetric measurements to study the reaction heats of catalytic CO oxidation on Pt surfaces. They calculated the expected heat for the initial reaction of CO with pre-adsorbed oxygen to be 180 ± 16 kJ mol^{-1}, which is close to the values measured in this study. As it was observed by TPR, temperatures higher than 100 °C are necessary for platinum reduction under hydrogen flow. Thus, it can be expected that after pretreatment under static hydrogen at room temperature, some weakly bound oxygen species remained on the catalyst surface and could react with the first CO doses.

Microcalorimetric measurements of the differential heats of hydrogen adsorption versus hydrogen coverage were also performed at 30 °C for the Pt/C catalysts. The adsorbed hydrogen uptakes on the various catalysts are summarized in Table 5.

Fig. 9 shows the differential heats of hydrogen adsorption versus adsorbate coverage on the Pt/C catalysts. The curves are roughly composed of two main regions. At the very beginning a sharp decrease of Q_{diff} is generally observed, which could be assigned to the adsorption on a few very strong sites or some remaining oxidized sites. In the next region a relatively slight decrease in Q_{diff} or even a short plateau is observed, corresponding to the heats released during adsorption on the predominant sites.

Table 5
Calorimetric data for hydrogen adsorption at 30 °C on the Pt/C-T, Pt/C-E, Pt/C-JM1 and Pt/C-JM2 catalysts.

Catalyst	Q_{diff}[a] (kJ mol^{-1})	Hydrogen uptake (μmol$_{H_2}$ g$_{Pt}^{-1}$)	
		n_{total}[b]	n_{irrev}[c]
Pt/C-T	72.9	513	125
Pt/C-E	72.3	502	110
Pt/C-JM1	75.2	551	72
Pt/C-JM2	73.4	41	3

[a] Differential heats calculated as average of the plateau values.
[b] Amount of H_2 adsorbed under an equilibrium pressure of 0.2 Torr.
[c] Amount of irreversibly chemisorbed H_2.

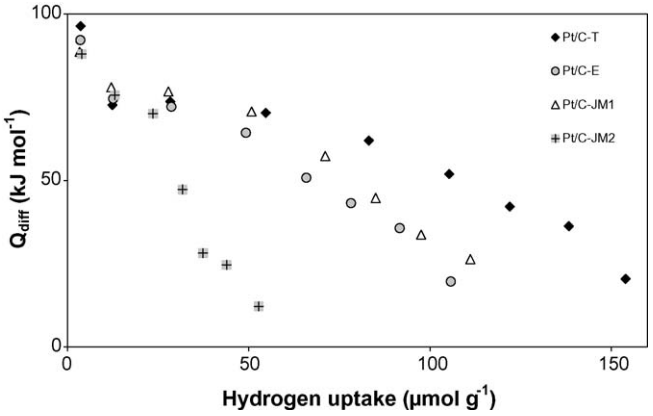

Fig. 9. Differential heats of hydrogen adsorption at 30 °C as a function of surface coverage for Pt/C-T, Pt/C-E, Pt/C-JM1 and Pt/C-JM2 catalysts.

For Pt/C-JM2 sample, the decrease of Q_{diff} with the adsorbed volume is more important. Similar initial heats of hydrogen adsorption are observed, with values of 98, 95 and 89 kJ mol^{-1} for Pt/C-T, Pt/C-E and Pt/C-JM, respectively, in good agreement with previously published values for supported and unsupported platinum catalysts. For example, Cerny et al. [73] estimated an initial heat of 89 kJ mol^{-1} for hydrogen adsorption at room temperature on evaporated platinum films. Lantz and Gonzales [74] and Herrmann et al. [75] reported values of 89 and 93 kJ mol^{-1} for hydrogen adsorption at around 30 °C on Pt/SiO_2 and Pt/TiO_2 catalysts, respectively.

It is worth noticing that the differential heats of CO adsorption are significantly higher than those found for hydrogen adsorption, indicating that CO would be adsorbed primarily in the case of possible competitive co-adsorption of these two gases. In addition, it can be seen from Tables 4 and 5 that the chemisorbed amount of CO is higher than the amount of chemisorbed H_2, which means that the investigated samples present a larger number of sites active for CO adsorption, in comparison with those active for hydrogen adsorption.

As shown in the experimental part, carbon monoxide was adsorbed on the catalysts previously contacted with H_2. Even if the samples were evacuated before CO adsorption, CO was adsorbed on a surface partly covered with strongly bonded hydrogen molecules which were not completely desorbed during outgassing under vacuum. As observed from the variation of the differential heats with CO uptake, up to CO coverage of about 100 μmol g^{-1} catalyst, the CO molecules are adsorbed on unoccupied active sites on the catalyst surface. Above this value an increase of differential heats was noticed and interpreted as the occurrence of CO adsorption over chemisorbed H_2. In addition to increasing differential heats a complex stepwise adsorption isotherm was observed (see Fig. 6) thus confirming a possible surface reaction between H_2 and CO. A possibility of reaction between pre-adsorbed hydrogen and CO has been already reported by Rush et al. [76] who found by using ^{13}C NMR of ^{13}CO adsorbed onto Pt in an acid electrolyte at ambient temperature three distinct forms of adsorbed CO: linear carbonyl (which is predominant as seen also by FTIR [69]), bridged carbonyl, and reduced carbonyl with the CHO stoichiometry. The latter reduced carbonyl occupies a single adsorption site and is formed upon adsorption in the presence of, and possibly through a reaction with, adsorbed hydrogen. It has been claimed in the literature [76–79] that, in addition to the dominant adsorbed CO species, a different chemical species (the nature of which is not known) is formed when CO adsorbs on the Pt surface in PEM fuel cells. The adsorbed species proposed so far are: Pt-COH, Pt-CHO, Pt-COOH, Pt-(CO_{ads})(OH_{ads}), or Pt-(CO_{ads})(H_2O_{ads}). It could be stated that in the case of CO adsorption over chemisorbed hydrogen, surface reactions happen as a result of competitive adsorption between previously adsorbed H_2 and incoming CO from the gas phase.

Concerning the stoichiometry of CO adsorption, is has to be pointed out that no attempt was made to verify it experimentally in this study, and the prescriptions found in the literature [42,43,66,80] have been followed. Gruber [80] has shown that for high platinum dispersion less than one CO is adsorbed for each surface platinum. Based on the well known fact that chemisorption of CO on platinum at room temperature can occur in two different forms (linear and bridged, according to infrared studies [69]) and using both CO and H_2 adsorptions, it is possible to calculate the proportion of CO adsorbed in the bridged structure. For instance, if all CO is adsorbed in linear form, then the ratio between the adsorbed CO and hydrogen amounts on the same catalyst, obtained in the same experimental conditions, is 2, while if for example 50% of adsorbed CO are present in the linear structure and 50% in the bridged structure, then the ratio becomes 1.33.

Using the CO and hydrogen uptakes obtained experimentally for the Pt/C catalysts investigated in this work, a CO/H_2 ratio of about 2 was calculated for all samples, and consequently a Pt:CO = 1:1 stoichiometry was assumed.

There are studies [81] which propose that the Pt:CO stoichiometry is a function of the metallic particle size, considering that the surfaces of small metal particles consist of adjoining faces which are parts of single crystal planes. A certain proportion of the total number of surface atoms in a small metal particle resides on edges and corners. Thus, the expected stoichiometry of adsorption for a small particle is determined by the proportion of different faces and by the possibility of multiple adsorption on edge and corner atoms. Following the method described by Ladas [81] and using the experimental results obtained in this study, the obtained stoichiometry of CO adsorption on the investigated Pt/C catalysts ranges between 0.5 and 0.6 for larger particles and increases for smaller particles. In this case similar metallic particle sizes of around 1.8 nm were obtained from microcalorimetric data for Pt/C-T, Pt/C-E and Pt/C-JM1 samples, in agreement with the XRD data.

From the measurements performed in this study, there is no doubt that CO adsorbs quickly and essentially irreversibly on Pt even in presence of pre-adsorbed hydrogen on the catalyst surface. Among the investigated samples, Pt/C-JM1 seems to be the most viable catalyst to be used for further fuel cell applications.

4. Conclusions

In this study it was proven that the adsorption microcalorimetry, although not widely used in this kind of work, is a powerful technique to study the effect of different pollutants on the anode and cathode sides of fuel cells. This technique was used to investigate the energetics of hydrogen and CO adsorption on Pt/C catalysts provided by various companies (Tanaka, E-Tek and Johnson Matthey) with possible application in PEMFCs.

The obtained microcalorimetric results showed that both H_2 and CO can be chemisorbed on the investigated samples. All the catalysts exhibited significantly higher differential heats of carbon monoxide adsorption in comparison with hydrogen adsorption, indicating that in case of co-adsorption of these two gases CO will be primarily adsorbed. A reaction between pre-adsorbed H_2 and CO from the gas phase was observed on Pt/C samples when a certain CO residual pressure was attained, as a result of competitive adsorption.

The CO adsorption capacity decreased for all investigated catalysts during successive air/H_2/CO cycles, due to the partial surface coverage of Pt particles by chemisorbed CO species. The

Pt/C catalyst provided by Johnson Matthey (16 wt.% Pt) was found to be the most tolerant to CO poisoning, with only 2% of the platinum surface blocked by irreversibly adsorbed CO molecules. The CO-poisoning degrees after 4 cycles were 10 and 13% for the E-Tek and Tanaka catalysts, respectively. These two catalysts present similar surface properties and the amount of CO adsorbed was found to be directly related to the Pt loading.

Concerning H_2 adsorption results, the Johnson Matthey powder (Pt/C-JM1) was the most efficient of the investigated catalysts: under the same experimental conditions it adsorbs the highest amount of hydrogen, with the smallest proportion of molecules irreversibly adsorbed.

Thus, the Pt/C-JM1 catalyst seems to be the most appropriate one for use in PEMFC applications.

Acknowledgements

The authors thank to Dr. G. Bergeret for XRD analysis, N. Cristin for isotherm measurements and the ANR (project ANR-06-PANH-002) for financial support.

References

[1] M. Yamawaki, T. Nishihara, Y. Inagaki, K. Minato, H. Oigawa, K. Onuki, R. Ogawa, Int. J. Hydrogen Energy 32 (2007) 2719–2725.
[2] H. Wendt, E.V. Spinacé, A. Oliveira Neto, M. Linardi, Quim. Nova 28 (6) (2005) 1066–1075.
[3] L. Carrette, K.A. Friedrich, U. Stimming, Fuel Cells 1 (2001) 5–39.
[4] C.-H. Wan, Q.-H. Zhuang, Electrochim. Acta 52 (2007) 4111–4123.
[5] H.F. Oetjen, V.M. Schmidt, U. Stimming, F. Trila, J. Electrochem. Soc. 143 (1996) 3838–3842.
[6] X. Cheng, Z. Shi, N. Glass, L. Zhang, J. Zhang, D. Song, Z.-S. Liu, H. Wang, J. Shen, J. Power Sources 165 (2007) 739–756.
[7] S.F. Yin, B.Q. Xu, X.P. Zhou, C.T. Au, Appl. Catal. A: Gen. 277 (2004) 1–9.
[8] H.A. Gasteiger, N. Markovic, P.N. Ross, E.J. Cairns, J. Phys. Chem. 98 (1994) 617–625.
[9] S. Wasmus, A. Kuver, J. Electroanal. Chem. 461 (1999) 14–31.
[10] T. Iwasita, Electrochim. Acta 47 (2002) 3663–3674.
[11] S. Gottesfeld, J. Pafford, J. Electrochem. Soc. 135 (1988) 2651–2652.
[12] L. Li, G. Wu, B.Q. Xu, Carbon 44 (2006) 2973–2983.
[13] K. Kolbrecka, J. Przyluski, Electrochim. Acta 39 (1994) 1591–1595.
[14] P. Liu, A. Logadottir, J.K. Norskov, Electrochim. Acta 48 (2003) 3731–3742.
[15] S. Desai, M. Neurock, Electrochim. Acta 48 (2003) 3759–3773.
[16] H.P. Dahr, L.G. Christner, A.K. Kush, J. Electrochem. Soc. 134 (1987) 3021–3026.
[17] B.N. Grgur, N.M. Markovic, P.N. Ross, Electrochim. Acta 43 (1998) 3631–3635.
[18] W. Vogel, J. Lundquist, P. Ross, P. Stonehart, Electrochim. Acta 20 (1975) 79–93.
[19] Z. Qi, C. He, A. Kaufman, Electrochem. Solid-State Lett. 4 (2001) A204–A205.
[20] Z. Qi, C. He, A. Kaufman, J. Power Sources 111 (2002) 239–247.
[21] G. Ertl, M. Neumann, K.M. Streit, Surf. Sci. 64 (1977) 393–410.
[22] P.A. Thiel, R.J. Behm, P.R. Norton, G. Ertl, J. Chem. Phys. 78 (1983) 7448–7458.
[23] M. Wasberg, L. Palaikis, S. Wallen, M. Kamrath, A. Wieckowski, J. Electroanal. Chem. 256 (1988) 51–63.
[24] D. Zurawski, M. Wasberg, A. Wieckowski, J. Phys. Chem. 94 (1990) 2076–2082.
[25] H. Steininger, S. Lehwald, H. Ibach, Surf. Sci. 123 (1982) 264–282.
[26] R.J. Behm, P.A. Thiel, P.R. Norton, G. Ertl, J. Chem. Phys. 78 (1983) 7437–7447.
[27] J. Liu, M. Xu, T. Nordmeyer, F. Zaera, J. Phys. Chem. 99 (1995) 6167–6175.
[28] N.J. Persson, M. Tushaus, A.M. Bradshaw, J. Chem. Phys. 92 (1990) 5034–5046.
[29] A. Guerrero-Ruiz, S.W. Yang, Q. Xin, A. Maroto-Valiente, M. Benito-Gonzales, I. Rodriguez-Ramos, Langmuir 16 (2000) 8100–8106.
[30] A. Guerrero-Ruiz, A. Maroto-Valiente, M. Cerro-Alarcon, B. Bachiller-Baeza, I. Rodriguez-Ramos, Top. Catal. 19 (2002) 303–311.
[31] A. Auroux, in: H. Karge, J. Weitkamp (Eds.), Molecular Sieves—Science and Technology: Acidity and Basicity, vol. 6, Springer Verlag, 2008, pp. 45–152.
[32] N. Cardona-Martinez, J.A. Dumesic, Adv. Catal. 38 (1992) 149–244.
[33] P.J. Anderson, H.H. Kung, Catalysis 11 (1994) 441–466.
[34] A. Auroux, in: B. Imelik, J.C. Vedrine (Eds.), Catalyst Characterization: Physical Techniques for Solid Materials, Plenum Press, New York, 1994, pp. 611–650.
[35] J. Silvestre-Albero, J.C. Serrano-Ruiz, A. Sepulveda-Escribano, F. Rodriguez-Reinoso, Appl. Catal. A: Gen. 292 (2005) 244–251.
[36] J.C. Serrano-Ruiz, A. Lopez-Cudero, J. Solla-Gullon, A. Sepulveda-Escribano, A. Aldaz, F. Rodriguez-Reinoso, J. Catal. 253 (2008) 159–166.
[37] A. Guerrero-Ruiz, P. Badenes, I. Rodriguez-Ramos, Appl. Catal. A: Gen. 173 (1998) 313–321.
[38] J.C. Serano-Ruiz, A. Sepulveda-Escribano, F. Rodriguez-Reinoso, J. Catal. 246 (2007) 158–165.
[39] J. Ruiz-Martinez, A. Sepulveda-Escribano, J.A. Anderson, F. Rodriguez-Reinoso, Catal. Today 123 (2007) 235–244.
[40] J.C. Serrano-Ruiz, G.W. Huber, M.A. Sanchez-Castillo, J.A. Dumesic, F. Rodriguez-Reinoso, A. Sepulveda-Escribano, J. Catal. 241 (2006) 378–388.
[41] D. Uner, M. Uner, Thermochim. Acta 434 (2005) 107–112.
[42] A. Maroto-Valiente, I. Rodriguez-Ramos, A. Guerrero-Ruiz, Themochim. Acta 379 (2001) 195–199.
[43] H. Kivrak, A. Mastalir, Z. Kiraly, D. Uner, Catal. Commun. 10 (2009) 1002–1005.
[44] R. Alcala, J.W. Shabaker, G.W. Huber, M.A. Sanchez-Castillo, J.A. Dumesic, J. Phys. Chem. B 109 (2005) 2074–2085.
[45] R.D. Cortright, J.A. Dumesic, J. Catal. 148 (1994) 771–778.
[46] R.D. Cortright, J.A. Dumesic, J. Catal. 157 (1995) 576–583.
[47] A. Ignaszak, S. Ye, E. Gyenge, J. Phys. Chem. C 113 (2009) 298–307.
[48] G. Ertl, H. Knozinger, F. Schuth, J. Weitkamp (Eds.), Handbook of Heterogeneous Catalysis second ed., 2008, p. 748.
[49] A. Erham Aksoylu, M. Madalena, A. Freitas, M. Fernando, R. Pereira, J.L. Figueiredo, Carbon 39 (2001) 175–185 (and references therein).
[50] A. Auroux, Top. Catal. 4 (1997) 71–89.
[51] A. Auroux, Top. Catal. 19 (2002) 205–213.
[52] G. Blyholder, R. Sheets, J. Phys. Chem. 74 (1970) 4335–4338.
[53] K.S.W. Sing, D.H. Everett, R.A.W. Haul, L. Moscou, R.A. Pierotti, J. Rouquérol, Pure Appl. Chem. 57 (1985) 603–619.
[54] V. Raghuveer, A. Manthiram, Electrochem. Solid-State Lett. 7 (2004) A336–A339.
[55] K.L. Yang, S. Yiacoumi, C. Tsouris, J. Electroanal. Chem. 540 (2003) 159–167.
[56] Y. Qian, W. Wen, P.A. Adcock, Z. Jiang, N. Hakim, M.S. Saha, S. Mukerjee, J. Phys. Chem. C 112 (2008) 1146–1157.
[57] M. Cerro-Alarcon, A. Maroto-Valiente, I. Rodriguez-Ramos, A. Guerrero-Ruiz, Carbon 43 (2005) 2711–2722.
[58] S. Haydar, C. Moreno-Castilla, M.A. Ferro-Garcia, F. Carrasco-Marin, J. Rivera-Utrilla, A. Perrard, J.P. Joly, Carbon 38 (2000) 1297–1308 (and references therein).
[59] J.L. Figueiredo, M.F.R. Pereira, M.M.A. Freitas, J.J.M. Orfao, Carbon 37 (1999) 1379–1389 (and references therein).
[60] J.A. Menéndez, J. Phillips, B. Xia, L.R. Radovic, Langmuir 12 (1996) 4404–4410.
[61] D.J. Ostgard, L. Kustov, K.R. Poeppelmeier, W.M.H. Sachtter, J. Catal 133 (1992) 342–357.
[62] H. Lieske, G. Lietz, H. Spindler, J. Volter, J. Catal. 81 (1983) 8–16.
[63] S.R. de Miguel, O.A. Scelza, M.C. Roman-Martinez, C. Salinas-Martinez de Lecea, D. Cazorla-Amores, A. Linares-Solano, Appl. Catal. A: Gen. 170 (1998) 93–103.
[64] D.A. Simonetti, E.L. Kunkes, J.A. Dumesic, J. Catal. 247 (2007) 298–306.
[65] J.A. Menéndez, L.R. Radovic, B. Xia, J. Phillips, J. Phys. Chem. 100 (1996) 17243–17248.
[66] C. Prado-Burguete, A. Linares-Solano, F. Rodriguez-Reinoso, C. Salinas-Martinez de Lecea, J. Catal. 128 (1991) 397–404.
[67] F. Rodriguez-Reinoso, I. Rodriguez-Ramos, C. Moreno-Castilla, A. Guerrero-Ruiz, J.D. Lopez-Gonzales, J. Catal. 99 (1986) 171–183.
[68] A.S. Gow, J. Phillips, Ind. Eng. Chem. Res. 31 (1992) 193–204.
[69] S.D. Jackson, B.M. Glanville, J. Willis, G.D. McLellan, G. Webb, R.B. Moyes, S. Simpson, P.B. Wells, R. Whyman, J. Catal. 139 (1993) 207–220.
[70] P. Gallezot, D. Richard, Catal. Rev. Sci. Eng. 40 (1998) 81–126.
[71] A. Guerrero-Ruiz, B. Bachiller-Baeza, I. Rodriguez-Ramos, Appl. Catal. A: Gen. 173 (1998) 231–238.
[72] C.E. Wartnaby, A. Stuck, Y.Y. Yeo, D.A. King, J. Chem. Phys. 102 (1995) 1855–1858.
[73] S. Cerny, M. Smutek, F. Buzek, J. Catal. 38 (1975) 245–256.
[74] J.B. Lantz, R.D. Gonzalez, J. Catal. 41 (1976) 293–302.
[75] J.M. Herrmann, M. Gravelle-Rumeau-Maillot, P.C. Gravelle, J. Catal. 104 (1987) 136–146.
[76] B.M. Rush, J.A. Reimer, E.J. Cairns, J. Electrochem. Soc. 148 (2001) A137–A148.
[77] Y. Zhu, H. Uchida, M. Watanabe, Langmuir 15 (1999) 8757–8764.
[78] B. Beden, C. Lamy, N.R. De Tacconi, A.J. Arvia, Electrochim. Acta 35 (1990) 691–704.
[79] P. Stonehart, Electrochim. Acta 18 (1973) 63–68.
[80] H.L. Gruber, J. Phys. Chem. 66 (1962) 48–54.
[81] S. Ladas, Surf. Sci. 175 (1986) L681–L686 (and references therein).